

XMM-Newton View of the Hubble Deep Field-North and Groth-Westphal Strip Regions

T. MIYAJI¹, R.E. GRIFFITHS¹, D. LUMB², V. SARAJEDINI³, and H. SIDDIQUI²

¹ Department of Physics, Carnegie Mellon University, 5000 Forbes Ave., Pittsburgh, PA 15213, USA

² Science Payload Technology Divn., Research and Science Support Dept. of ESA ESTEC, 2200 AG Noordwijk, The Netherlands

³ Department of Astronomy, University of Florida, Gainesville, FL 32611-2055, USA

Received date will be inserted by the editor; accepted date will be inserted by the editor

Abstract. We report the progress on our analysis of two deep XMM observations in the areas of Hubble Deep Field-North and the Groth-Westphal Strip field. We present the source detection method, Monte-Carlo simulation on source detection, and our preliminary $\text{Log } N - \text{Log } S$ relations. Comparing these two fields and other fields in literature, we find up to $\sim 30\%$ variations in number counts near our flux limits, which is most likely to be due to cosmic variance. This serves as a pilot study for a more systematic investigation. The nature of the X-ray sources in the Groth-Westphal field is also discussed in terms of hardness ratios, morphology and spectroscopic properties.

Key words: galaxies:active – (galaxies:)quasars:general – surveys – X-rays

1. Introduction

With the large collecting area and field of view, XMM-Newton provides complementary probe to the faint X-ray source population to the Chandra X-ray observatory. With a relatively short exposure, it collects sufficient photons to provide decent X-ray spectroscopy. Because of the limited fields of view in the Chandra Deep Fields North and South, collecting intermediate exposure XMM-Newton observations can probe the behavior of the X-ray sources at several $\sim 10^{-16}$ [erg s⁻¹ cm⁻²] (0.5-2 keV) or several $\sim 10^{-15}$ [erg s⁻¹ cm⁻²] (2-10 keV) with fair sampling of the universe.

In this proceedings article, we report our progress on the analysis of two deep surveys using XMM-Newton, one on the Hubble Deep Field-North and surroundings (HDF-N) and the other on the Groth-Westphal Strip field (GWS). These fields have originally been selected because of the abundance of multiwavelength data. We note that the HDF-N field has the deepest Chandra observation (the Chandra Deep Field-North, e.g. Alexander et al. this volume) and a part of the GWS has 200 ks of Chandra observations. Because of the depth of these observations, Chandra observations can provide better quality data than these XMM-Newton observations for most purposes. However, we use these data as training sets for investigating source detection properties with XMM-Newton and

to extend the source count investigation on multiple fields to investigate the effects of the large scale structure of the universe. Also the XMM field of view of the GWS is much larger than the single-pointing Chandra observation. Thus XMM-Newton still provides the only source of X-ray data for a significant part of the Groth Strip itself, consisting of 28 contiguous Hubble Space Telescope Wide Field Planetary Camera 2 (HST WFPC2) imaging observations, out of which 16 are within the XMM-Newton FOV.

2. The XMM-Newton Observation

The X-ray data presented here are from guaranteed time (GT) programs of XMM-Newton. The observation log is shown below with the number of detected sources (within the central 11') and approximate flux limits.

Table 1. The Log of Observations and Detected Sources

Field	Expo. [ks]		$N_{\text{src}}(S_{\text{lim}}[\text{erg s}^{-1} \text{cm}^{-2}])$		
	PN	MOS	0.5-2 keV	2-10 keV	5-10 keV
HDF-N	155	180	158 (4 10^{-16})	116 (2 10^{-15})	49 (4 10^{-15})
GWS	65	80	117 (6 10^{-16})	91 (4 10^{-15})	35 (6 10^{-15})

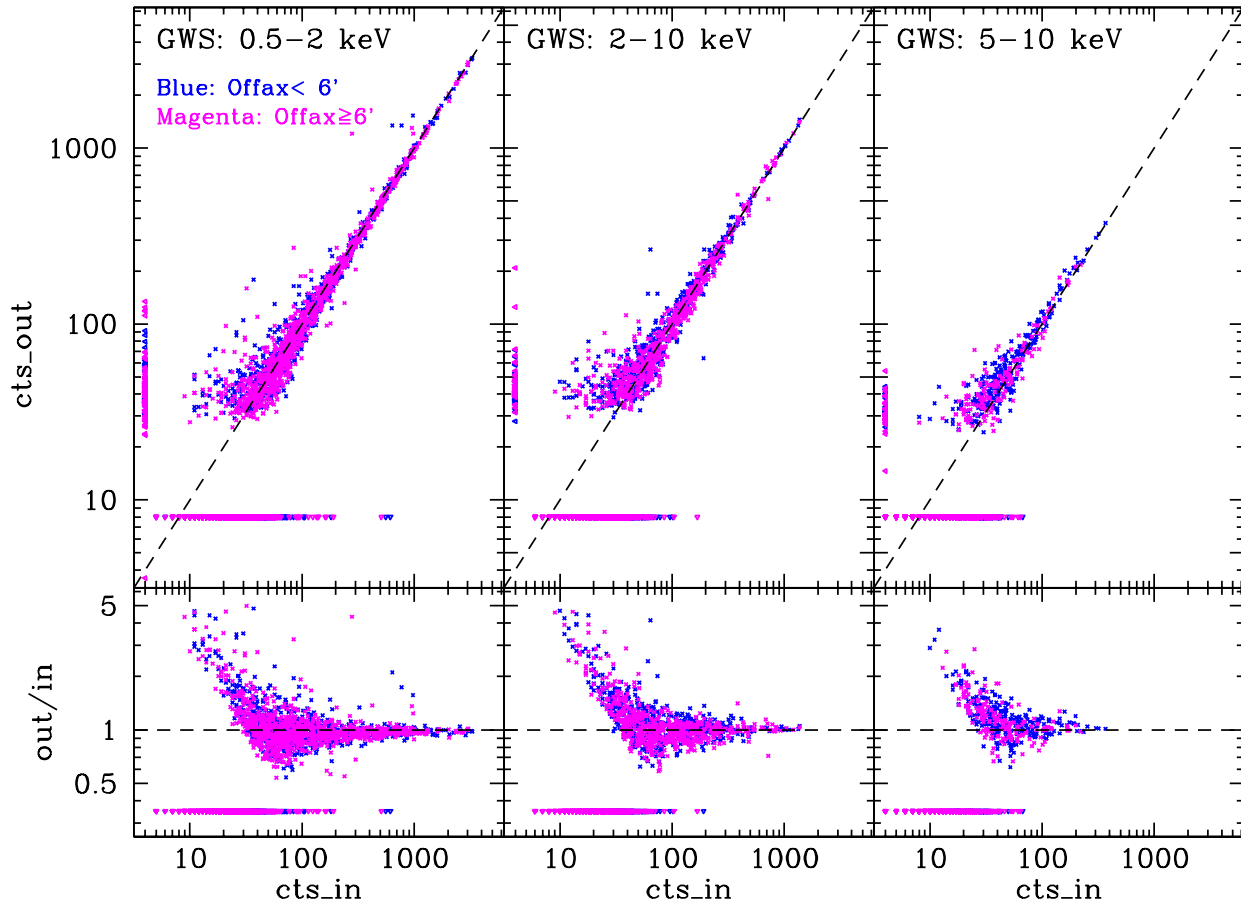


Fig. 1. The source counts detected in the source detected chain are plotted against the input counts for the Monte-Carlo simulations corresponding to the XMM-Newton observations of GWS in three energy bands as labeled. In the electronic version, the source within $< 6'$ from the optical axis are plotted in blue points, while those outside in magenta. Also the ratio of output and input counts are shown.

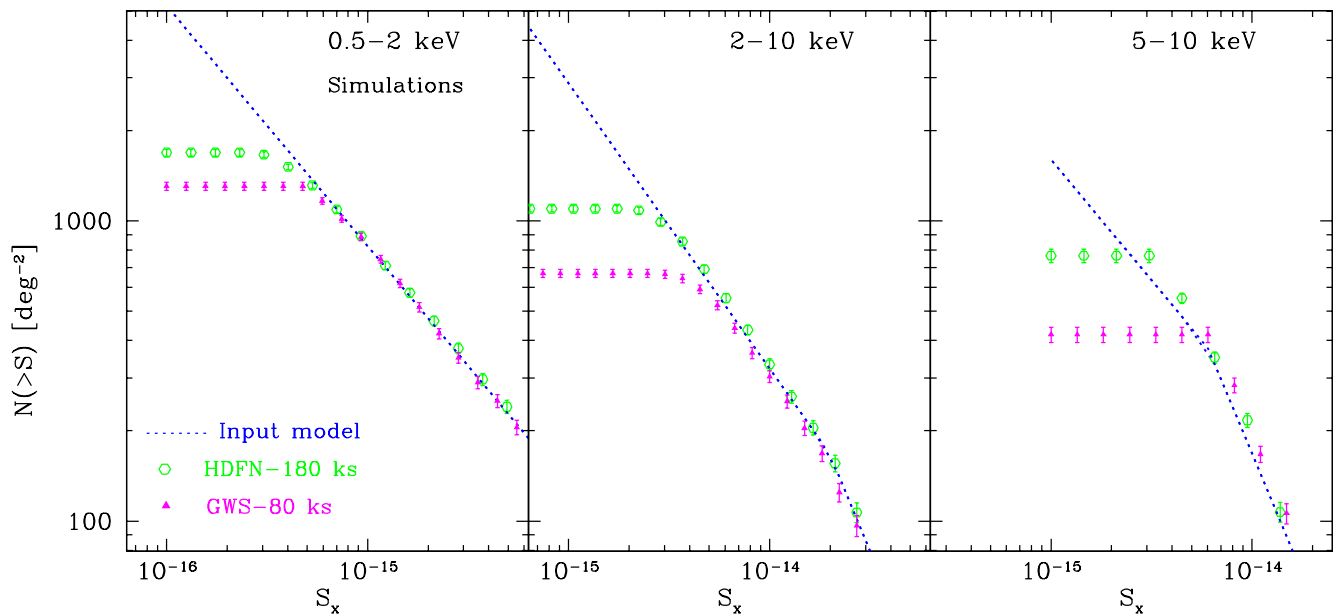


Fig. 2. The input $\text{Log } N - \text{Log } S$ relation assumed for the Monte-Carlo simulations (dotted lines) are compared with those derived from the source detection procedure described in the text, assuming a uniform sensitivity over the field

3. Source Detection and $\text{Log } N - \text{Log } S$

We have performed source detection using the SAS procedure to the sum of the PN and two MOS detectors. The exposure map has been summed by weighting using PN and MOS responses in each band (assuming a $\Gamma = 1.4$ power-law). We have first used *eboxdetect* in the local detect mode. We then created a smoothed background map using the *esplinemap*, which gives a spline fitted image in the source excluded map. This is followed by another *eboxdetect* run in the map detect mode, where the sliding box cell searches for excesses over the smoothed background map. Finally, the task *emldetect* has been applied to make maximum-likelihood fitting to the candidate source positions. We have treated sources with the likelihood value of $ML = -\ln(1 - P) > 14$, where P is the probability that the source exists.

There is a caveat in this source detection procedure. Depending on the selection of parameters such as the number of spline nodes, *esplinemap* often gives spurious wavy features, which give rise to a concentration of spurious sources or a void of detected sources. Currently we manually search for *espline* parameters which gives best results. This will be improved in the future.

The inner 9.6 arcminute region has been used for the $\text{Log } N - \text{Log } S$ analysis. In order to assess the limiting flux-area relation and incompleteness, we have made Monte-Carlo simulation using our multi-purpose image simulator *qimsim* (see Miyaji & Griffiths 2002a). The simulated images have been processed through the same source detection procedure. Fig.1 compares input and detected photon counts for the simulation runs corresponding to the GWS observations. At the brightest end, the input and output counts match quite well, even though the point spread functions used in the simulations and those for the *emldetect* correspond to different calibrations. This shows that the counts in the source detection is not very sensitive to the PSF calibration. We expect that the spread about the $\text{cts}_{\text{out}} = \text{cts}_{\text{in}}$ line decreases as we use an improved method for the background map generation (e.g. Baldi et al. 2002). Fig.2 shows the input $\text{Log } N - \text{Log } S$ relations and those calculated from detected sources assuming a limiting flux corresponding to constant count over the field. Fig.2 shows incompleteness near the flux limit. Eddington bias can be seen in the 5-10 keV band, where the input $\text{Log } N - \text{Log } S$ is still steep at the limiting flux.

Fig.3 shows the preliminary results, after first-order correction for incompleteness and Eddington bias using the results of the simulation. Further corrections similar to that of Moretti et al. (2002), which involves mapping of detected photon counts to incident counts for each source, will be applied in a future full-length paper. We also overplot the curves from XMM-Newton observation of the Lockman Hole (Hasinger et al. 1993) and of the inner part of the Chandra Deep Field North with fluctuation analysis results (Miyaji & Griffiths 2002a). In the 5-10 keV plot, the results from HELLAS2XMM is also shown. We observe the variation of 20-30% at the limiting fluxes of our XMM-Newton observation, which is most likely to be caused by the cosmic variance.

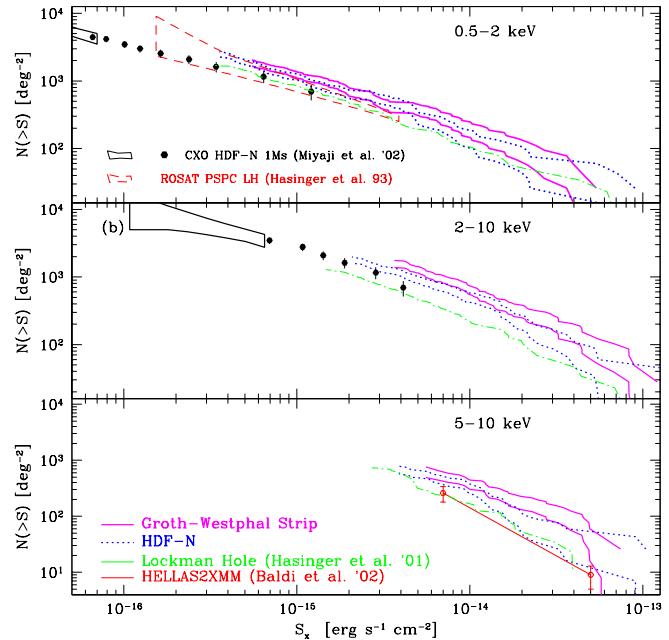


Fig. 3. The $\text{Log } N - \text{Log } S$ relations are plotted in the 0.5-2keV (soft), 2-10 keV (hard) and 0.5-10 keV (ultrahard) bands respectively for the XMM observations of HDF-North and Groth-Westphal fields respectively. The upper and lower curves show $\pm 1\sigma$ range. The results of a number of other sources are also shown as labeled.

4. X-ray Sources in the Groth-Westphal Field

In this section, we report the properties of the X-ray sources detected in the GWS field. We concentrate on the 24 sources within the HST WFPC2 fields of view, where the DEEP¹ redshift survey is also concentrated. A more extensive redshift survey (DEEP2²) has started, which will cover most of the XMM-Newton field of view. This field is also a subject of the SIRTf legacy program, a planned target of the GALEX mission, and many other existing and future programs, which leaves potential for unique studies of the X-ray source population.

Out of the 24 XMM-Newton sources, 10 have spectroscopic redshifts from the DEEP survey and 5 have photometric redshifts (Brunner et al. 2000). Out of the 10 spectroscopically identified sources, two clearly have broad lines indicative of type 1 AGN, two have no broad permitted lines but show high excitation lines indicative of Seyfert 2 activity. The rest have narrow emission lines with no clear AGN indication. Using the HST Medium Deep Survey (MDS) database³, giving bulge/disk decomposition, we can immediately find the morphological properties of these sources as shown in Table 2. Fig. 4 shows X-ray color-color diagram of these 24 sources with spectroscopic and morphological properties overlaid.

In spite of the small number, we see some trends. Sources are distributed along the grid, showing that absorbed power-

¹ <http://deep.ucolick.org/>

² <http://astron.berkeley.edu/davis/deep/>

³ <http://archive.stsci.edu/mds/>

Table 2. MDS Morphologies of X-ray sources

Stellar	Disk+Bulge	Pure Bulge	Galaxy ^{a)}	No MDS
3	2	3	2	2

a) An extended component has been resolved but the galaxy is too faint for a disk/bulge discrimination.

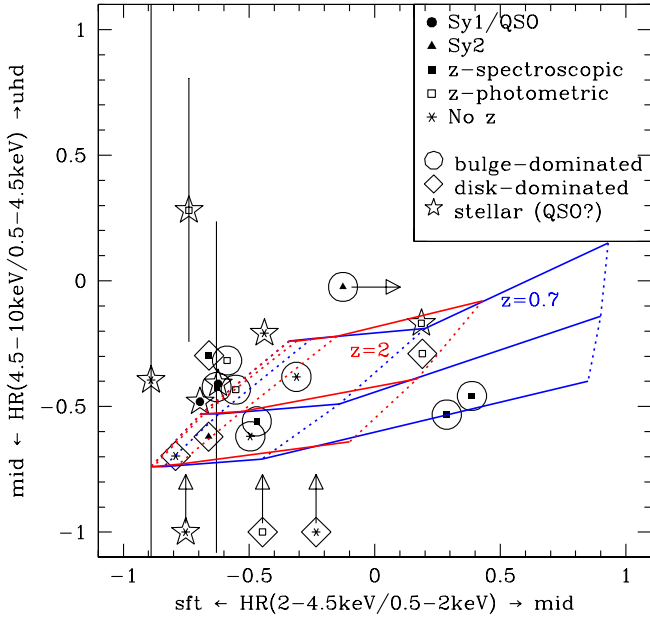


Fig. 4. The X-ray color-color diagram of the 24 X-ray sources. The inner symbol show spectral classification and the outer symbol show the morphological classification as labeled. Typical 1σ errors are 0.05-0.2 and error bars are shown for those larger than 0.4. The grid shows the location for absorbed power-law spectra for $z=0.7$ (wider grid, shown in blue for the electronic version) and $z=2$ (narrower grid, shown in red for the electronic version). The solid lines correspond to photon indices of $\Gamma = 1, 2,$ and 3 from top to bottom and the dotted lines to $\text{Log}N_{\text{H}} = -\infty, 21.5, 22.5,$ and 23.5 cm^{-2} from left to right respectively.

law is a good description of most sources. This can be seen with direct spectra of these sources (Miyaji & Griffiths 2002b). We also note two bulge-dominated (elliptical) sources with the hardest HR1, both of which are located at $z \sim 0.7 - 0.9$, and with no apparent sign of AGN activity. In order to search for signs of AGN activity, we plan to observe ~ 10 galaxies at $z > 0.7$ with Subaru OHS infrared spectrometer aiming at redshifted $\text{H}\alpha$ and [NII] emission lines. The proposal has been accepted and the observation is expected to be in early 2003. We aim to find hidden AGN activity in the X-ray sources which only show normal galaxy characters in their optical spectra.

5. Conclusion

In this proceedings paper, we have reported the progress of our analysis on deep XMM-Newton observations of the HDF-N and GWS fields. We have described the source detec-

tion procedures, Monte-Carlo simulations, and resulting $\text{Log } N - \text{Log } S$ relations in 0.5-2, 2-10, and 5-10 keV bands. Comparing the results from these two fields as well as other works, we see the variations of source density of $\sim 30\%$ near our flux limit, which is most likely to be due to cosmic variance. With XMM-Newton, a more systematic study is possible by collecting archival data of the fields with similar depths.

Currently our analysis on the GWS field is concentrated on the overlap with the WFPC2 strip, where the DEEP project has been concentrated. With the abundance of morphological data from the HST MDS, we can add insights into the nature of the X-ray sources. With our planned near-infrared spectroscopy using the OHS spectrograph attached to the Subaru 8.2m telescope, we expect to find indications of an AGN activity in X-ray sources which look normal galaxies in the current optical data. We also can extend our spectroscopic identification with the DEEP2 program, which will cover most of the XMM-Newton FOV of GWS.

Acknowledgements. The authors acknowledge NASA grants NAG 5-10875 (LTSA) to TM and NAG 5-7423 to REG.

References

- Baldi, G. et al.: 2001, A&A 365, L45
- Brunner, R.J. et al. 2000, ApJ 541, 527
- Hasinger, G. et al.: 2001, A&A 365, L45
- Miyaji, T., Griffiths, R.E.: 2002a, ApJ 564, L5
- Miyaji, T., Griffiths, R.E.: 2002b, in Galaxy Clusters and the High Redshift Universe Observed in X-rays, eds. Neumann, D.M. & J. Trahn Than Van, (Saclay:CEA)
- Moretti, A., Lazzatti, D., Campana, S. Tagliaferri, G.: 2002, ApJ 570, 502